


Article

Borosilicate Glass-Ceramics Containing Zirconolite and Powellite for RE- and Mo-Rich Nuclear Waste Immobilization

Wei Wan ¹, Yongchang Zhu ^{2,*} , Xingquan Zhang ^{3,*}, Debo Yang ², Yonglin Huo ¹, Chong Xu ¹, Hongfu Yu ¹, Jian Zhao ¹, Jichuan Huo ¹ and Baojian Meng ²

- ¹ Fundamental Science on Nuclear Wastes and Environmental Safety Laboratory, Southwest University of Science and Technology, Mianyang 621010, China; wanwei992695714@163.com (W.W.); hyl20201016@163.com (Y.H.); yjcbma@163.com (C.X.); yuhongfu2018@mails.swust.edu.cn (H.Y.); z18210433040@163.com (J.Z.); huojichuan@swust.edu.cn (J.H.)
- ² China Building Materials Academy, Beijing 100024, China; yangdebo19770904@126.com (D.Y.); Baojian_meng@163.com (B.M.)
- ³ School of Materials Science and Engineering, Southwest University of Science and Technology, Mianyang 621010, China
- * Correspondence: zhuyongchang@cbma.com.cn (Y.Z.); zhangxingquan@swust.edu.cn (X.Z.); Tel./Fax: +86-65794978 (Y.Z.); +86-816-6089508 (X.Z.)

Abstract: In order to increase the loading of rare earth- and molybdenum-rich high-level waste in the waste forms, zirconolite- and powellite-based multi-phase borosilicate glass-ceramics were synthesized via an in-situ heat treatment method. The effects of the CTZ (CaO, TiO₂ and ZrO₂) content on the crystallization, microstructure and aqueous durability of the multi-phase borosilicate glass-ceramics were studied. The results indicate that the increase of CTZ content can promote crystallization. The glass-ceramics presented even structures when the CTZ content was ≥ 40 wt%. For the glass-ceramic with 40 wt% CTZ, only zirconolite and powellite crystals were detected and powellite crystals were mainly distributed around zirconolite, whereas for the glass-ceramics with 50 wt% CTZ, perovskite was detected. Furthermore, the leaching rates of Na, Ca, Mo and Nd were in the $\times 10^{-3}$, $\times 10^{-4}$, $\times 10^{-3}$ and $\times 10^{-5}$ g·m⁻²·d⁻¹ orders of magnitude on the 28th leaching day, respectively.

Keywords: multi-phase glass-ceramics; in situ heat treatment; zirconolite; powellite



Citation: Wan, W.; Zhu, Y.; Zhang, X.; Yang, D.; Huo, Y.; Xu, C.; Yu, H.; Zhao, J.; Huo, J.; Meng, B. Borosilicate Glass-Ceramics Containing Zirconolite and Powellite for RE- and Mo-Rich Nuclear Waste Immobilization. *Materials* **2021**, *14*, 5747. <https://doi.org/10.3390/ma14195747>

Academic Editor: Marta Miola

Received: 11 August 2021

Accepted: 27 September 2021

Published: 1 October 2021

Publisher's Note: MDPI stays neutral with regard to jurisdictional claims in published maps and institutional affiliations.



Copyright: © 2021 by the authors. Licensee MDPI, Basel, Switzerland. This article is an open access article distributed under the terms and conditions of the Creative Commons Attribution (CC BY) license (<https://creativecommons.org/licenses/by/4.0/>).

1. Introduction

Nuclear energy as a net-zero carbon emission energy source brings convenience to industry and life, but a large amount of spent fuel is produced in the process of producing nuclear energy. Different countries have different ways of disposing of spent fuel. Some countries, including the US, Canada and Sweden, have decided to leave their spent fuel in interim storage, whereas other countries such as France, Russia, the UK and Japan reprocess their spent nuclear fuel in order to recycle U and Pu that is used in new nuclear fuel and to reduce the radiotoxicity of the ultimate waste [1–3]. China has also decided to reprocess spent fuel. The reprocessing of spent fuel will produce a large quantity of high-level waste (HLW) containing rare earths (RE), minor actinides, transition metals, alkalis, alkaline earths and other fission products [4,5]. Most importantly, there are many radionuclides in HLW, which have strong radiotoxicity and can cause heritable damage to the organism. Once these radionuclides spill, they will have a devastating impact on the biosphere. Currently, how to immobilize HLW safely is a hot topic for researchers.

In order to immobilize the waste streams safely, researchers have developed a series of waste forms such as alleged crystal-free glass, ceramics and glass-ceramics [6]. Vitrification is the most widely used HLW immobilization disposal method around the world [7] and has been successfully commercialized. At present, the solubility of HLW in glass is about 15 wt%–20 wt% [1]. However, the low solubility of MoO₃ in borosilicate glass [8–16], due

to its high field strength, limits the high-level radioactive waste loading in borosilicate glass [17]. These molybdates may precipitate out in the process of the melt cooling or heat treatment of glass. Although Mo is a kind of non-radioactive fission product, it tends to form molybdates with poor durability such as Na_2MoO_4 and $^{137}\text{Cs}_2\text{MoO}_4$ (known as yellow phase). A large number of studies about molybdate have been reported [15,18,19], but there is still no significant increase in HLW loading in glass waste forms. For these reasons, glass-ceramics have been developed and are regarded as potential materials to immobilize fission products so as to increase the HLW loading.

Research has been conducted to increase the HLW loading. For example, the US Department of Energy (DOE) developed a new glass-ceramic waste form containing oxyapatite, powellite and rare earth borosilicate crystals to immobilize the fission products. These glass-ceramics with stable crystalline phases are deemed to be the ideal materials for RE- and Mo-rich HLW immobilization [6,20,21]. Based on this knowledge, much research has been conducted. McCloy reported the effects of different components on the glass structure and crystallization [6]. Crum reported the effects of in situ heat treatment at different temperatures on the crystallization of glass-ceramics [1]. Neeway et al. evaluated the dissolution kinetics of oxyapatite and powellite at different pH and the chemical stability of glass-ceramics prepared at different cooling rates [22,23]. Even the influence of the size of rare-earth ions on the phase evolution of Mo-containing glass-ceramics has been considered [13]. The loading of Nd_2O_3 in glass-ceramics containing oxyapatite is apparently higher than that of glass waste forms. However, McCloy [6] and Patil [13] also reported uncontrolled crystallization and surface crystallization of oxyapatite, which may cause uncertainty in the leaching behavior. Moreover, the anti-irradiation property of oxyapatite is not particularly suitable [24]. Therefore, developing new glass-ceramic waste forms to immobilize HLW is imperative.

Zirconolite ($\text{CaZrTi}_2\text{O}_7$) as a stable mineral found in nature has been extensively studied by scientists [25–27]. Due to its good chemical stability and thermal and irradiation properties, zirconolite is regarded as the crystalline phase with the most potential for HLW immobilization [28]. Zirconolite can be synthesized by adding relatively high amounts of TiO_2 and ZrO_2 into the glass as nucleating agents and then combining them with the corresponding heat treatment. Previous studies revealed that RE cations can replace both Ca^{2+} and Zr^{4+} sites of zirconolite structure [2,29], which enables RE to exist in the lattice of zirconolite, forming a stable crystalline phase. In addition, Loiseau reported that Nd^{3+} and Gd^{3+} can replace more than 60% of the Ca^{2+} sites of zirconolite without any structure distortion [30]. Therefore, zirconolite is considered a suitable material for Nd^{3+} immobilization. With zirconolite as a target crystal used for the immobilization of Nd_2O_3 , the optimal content of CTZ should be ascertained because an insufficient amount of zirconolite cannot provide enough sites for Nd, or superfluous CTZ content causes uncontrollable crystals and more unnecessary grain boundaries. Early zirconolite glass-ceramics were synthesized by the two-step method [30–32], which enabled glass melts to cool and then be reheated to nucleation and crystallization temperature. However, this process is not suitable for engineering because of its complex operation process. According to the DOE plan, the best way to achieve HLW immobilization is to accomplish the technological process in canisters, which allows the target crystals to form in one step. In order to maximally simplify the heat treatment process, this study was designed to synthesis the glass-ceramics containing zirconolite and powellite by in situ thermal treatment.

In consideration of the high content of RE and Mo, developing multi-phase glass-ceramic waste forms containing zirconolite and powellite is extremely urgent. Zirconolite for RE and powellite for Mo both exhibit good chemical durability. For example, the normalized leaching rates of zirconolite and powellite are generally below $\times 10^{-4}$ and $\times 10^{-2} \text{ g}\cdot\text{m}^{-2}\cdot\text{d}^{-1}$ orders of magnitude after 28 d, respectively [22,33]. Glass-ceramic waste forms used in engineering should have good microstructures and uniformity. For example, the grain size is within the acceptable range and evenly distributed, which is strongly related to composition and heat treatment. In order to maximally simplify the

preparation process of glass-ceramics, in situ heat treatment was performed. Therefore, the key is the composition of the glass-ceramics, especially the content of CTZ.

In this study, according to the 35 wt% HLW loading required by the national defense program, RE and Mo are considered key elements. All the RE included in HLW are replaced by Nd since their particle radiuses and chemical properties are similar. In order to study the effects of CTZ content on the crystalline phases, microstructure and aqueous durability of multi-phase borosilicate glass-ceramics containing zirconolite and powellite, a series of multi-phase borosilicate glass-ceramics containing zirconolite and powellite with different CTZ content were synthesized to immobilize the RE and Mo of HLW generated from a nuclear power plant in China by in situ heat treatment. This paper aims to (1) understand the relationship between CTZ content and the crystalline phase, microstructure and bulk density of the multi-phase borosilicate glass-ceramics, (2) determine the composition of the multi-phase glass-ceramic waste forms with optimum CTZ content and (3) evaluate the durability of the multi-phase glass-ceramics.

2. Experimental Procedures

Glass-ceramics containing different CTZ content were synthesized using a reagent grade of SiO₂, H₃BO₃, Na₂CO₃, Al(OH)₃, CaCO₃, TiO₂, ZrSiO₄, Nd₂O₃ and MoO₃ as raw materials. In order to study the effects of CTZ content on the crystallization, microstructure and chemical stability of multi-phase glass-ceramics, different levels of CTZ content (20, 30, 40 and 50 wt%) were added. It should be noted that CaCO₃ was designed to be divided into two parts, one for participating in the glass network and the formation of powellite crystals, the other part participating in the formation of zirconolite crystals. Table 1 shows the detailed compositions. All the ingredients were mixed and then held at 850 °C for 2 h to release carbon dioxide, before being melted in alumina crucibles at the temperature of 1250 °C for 3 h. All glass melts were poured into water, dried, ground into powder and reheated to 1250 °C for 2 h before in situ thermal treatment (slow cooling rate at about 5 °C·min⁻¹). The process of glass-ceramics synthesis is shown in Figure 1. The main ingredients of HLW are RE (27.02 wt%) and Mo (13.28 wt%), which account for a large proportion of the total mass. Thus, the key point of HLW immobilization can be simplified as the immobilization of Nd and Mo.

Table 1. Compositions of glass matrix (mol%).

	SiO ₂	B ₂ O ₃	Na ₂ O	Al ₂ O ₃	CaO	TiO ₂	ZrO ₂	Nd ₂ O ₃	MoO ₃
CTZ-20	48.80	10.73	12.07	1.21	7.63	7.83	3.41	2.67	3.07
CTZ-30	43.85	9.64	13.16	1.08	9.04	12.07	5.25	2.75	3.15
CTZ-40	38.63	8.50	11.60	0.95	10.53	16.53	7.19	2.82	3.24
CTZ-50	33.11	7.28	9.94	0.82	12.11	21.26	9.25	2.90	3.33

In order to confirm the glass transition temperature (T_g) as well as crystallization temperature (T_c), the quenched glass samples were tested by differential thermal analysis (DTA, SDT Q600, TA Instruments Inc., New Castle, DE, USA) with a heating rate of 20 °C·min⁻¹ in the air. All these samples were measured from room temperature to 1000 °C. The amorphous and crystalline phases of the glass-ceramics were identified by X-ray Diffraction (XRD, PANalytical X'Pert Pro diffractometer, Eindhoven, Holland) using Cu K α radiation, operating at 40 kV and 40 mA, ranging from 3° to 80°. The microstructure and element distribution of the glass-ceramics were identified using a scanning electron microscope (SEM, Ultra-55, ZEISS Company, Jena, Germany) and energy-dispersive X-ray spectroscopy (EDS, IE450X-Max80, Oxford Instruments Analytical Limited, Oxford, UK). The densities of the samples were measured by the pycnometer method. All samples were dried in an 80 °C oven for 2 h until the mass did not change. The following formula (1) is used to calculate the density of the sample and repeated 3 times to take the average (g·cm⁻³):

$$\rho_0 = \frac{m_0}{m_0 + m_1 - m_2} \times \rho_1 \quad (1)$$

where m_0 is the mass of the dry sample to be measured (g), m_1 is the mass of the pycnometer filled with deionized water (g), m_2 is the mass of the pycnometer filled with deionized water and the added sample (g) and ρ_1 is the density of water that is decided by its temperature ($\text{g}\cdot\text{cm}^{-3}$).

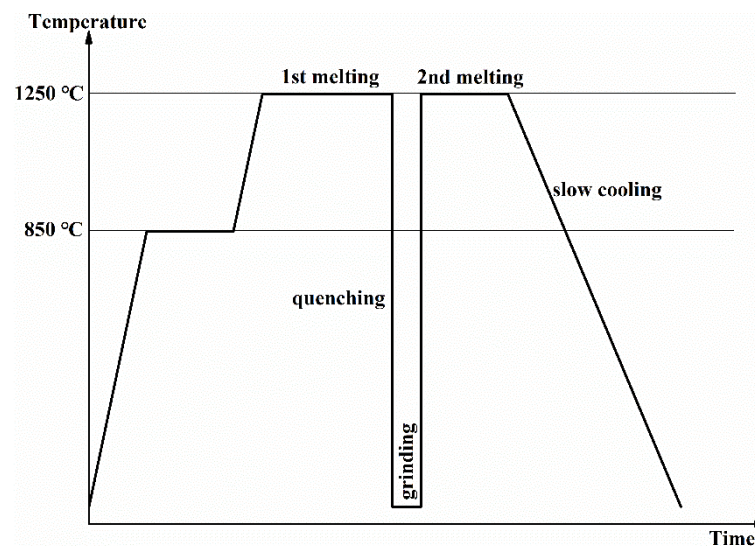


Figure 1. Schematic diagram of different stages of glass-ceramics preparation.

The chemical durability of the obtained glass-ceramic samples was investigated at 90 ± 1.0 °C in deionized water (pH = 7) in PTFE reactors, according to the Product Consistency Test (PCT) [34]. Glass-ceramics were ground into powder and passed through a 100–200 mesh sieve, cleaned with absolute ethanol and dried. Then, a 3 g sample was soaked in 80 mL of deionized water in a PTFE reactor at 90 ± 1.0 °C [29]. After 1, 3, 7, 14 and 28 days, the leachates were removed for measurement and 80 mL of fresh deionized water was added to the PTFE. Inductively coupled plasma-optical emission spectroscopy (ICP-OES, iCAP6500, Thermo Fisher Company, Waltham, MA, USA) and inductively coupled plasma-mass spectrometry (ICP-MS, 7700X, Agilent Technologies, Santa Clara, CA, USA) were performed to test the obtained leachate. The normalized leaching rate LR_i ($\text{g}\cdot\text{m}^{-2}\cdot\text{d}^{-1}$) was calculated according to the formula (2):

$$LR_i = \frac{C_i \cdot V}{f_i \cdot S \cdot \Delta t} \quad (2)$$

where C_i is the concentration of element i in the leachate ($\text{g}\cdot\text{L}^{-1}$), f_i is the mass fraction of the element i in the sample, Δt is the interval leaching duration in days (d), V is the volume of the leachate (L) and S is the surface area of the sample (m^2).

3. Results and Discussion

Figure 2 shows the DTA curves of the glass with different CTZ content. The T_g values of CTZ-20, CTZ-30, CTZ-40 and CTZ-50 are 605 °C, 654 °C, 661 °C and 667 °C, respectively. The result is similar to Li's [32]. For the CTZ-20 sample, there are two weak exothermic peaks at around 725 °C and 940 °C. The peak at around 940 °C corresponds to the crystallization of powellite [16]. In addition, the DTA curves of CTZ-30, CTZ-40 and CTZ-50 are similar. All of the above have two exothermic peaks at around 776 °C and 941 °C, which corresponds to the crystallization of zirconolite [17] and powellite phase, respectively, and the peak at 776 °C strengthened with the increasing content of CTZ. Additionally, the peak at 725 °C disappeared when the CTZ content increased to 30 wt%–50 wt%, which demonstrated that 20 wt% CTZ content cannot meet the requirements of zirconolite crystallization,

and another crystalline phase formed. The results indicate that an increase in CTZ content is beneficial to the crystallization of multi-phase glass-ceramics.

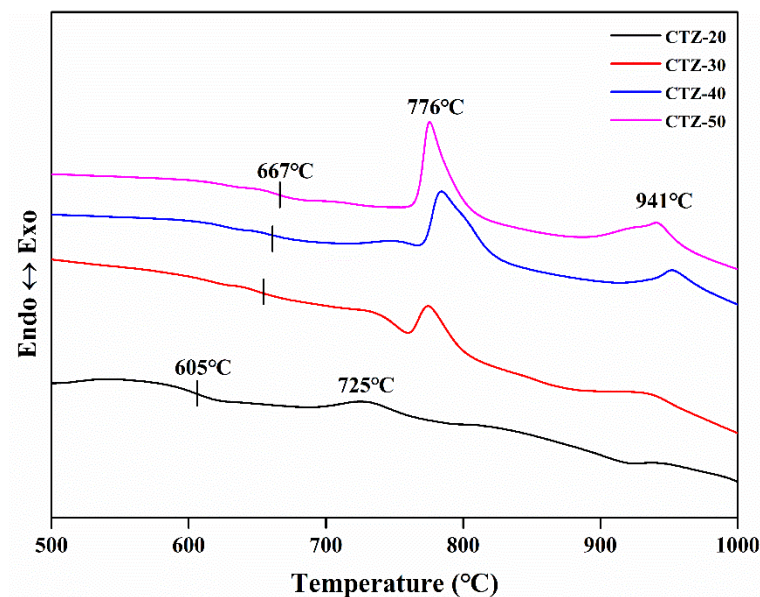


Figure 2. DTA curves of the glass with different CTZ content.

Figure 3 presents the XRD patterns of the glass-ceramics. For the CTZ-20 sample, it can be seen that the main crystalline phase is neodymium aluminum perovskite (NdAlO_3 , PDF#76-1336) [35], and the weak characteristic peaks belonging to powellite (CaMoO_4 , PDF#85-0585) and zirconolite ($\text{CaZrTi}_2\text{O}_7$ -2M, PDF#84-0163) were also observed. This is because low CTZ content is not conducive to the crystallization of zirconolite. When the CTZ content increases, intense characteristic peaks belonging to zirconolite and powellite are observed in the CTZ-30, CTZ-40 and CTZ-50 samples. It is interesting to note that no neodymium aluminum perovskite crystals were detected in these glass-ceramics. This may be because the increase in CTZ content leads to an increase in, and during the crystallization of zirconolite, Nd^{3+} cations entered its lattice, resulting in the disappearance of neodymium aluminum perovskite in the samples. For the CTZ-30 and CTZ-40 samples, only two target crystalline phases for zirconolite and powellite were observed. However, the intense characteristic peaks belonging to perovskite (CaTiO_3 , PDF#81-0562) were detected in the CTZ-50 sample. This is because excessive TiO_2 leads to the formation of perovskite, which is similar to what Wu reported [36]. These results are consistent with those of DTA. In conclusion, the CTZ-30 and CTZ-40 samples meet the experimental design based on the purpose of preparing multi-phase glass-ceramics containing zirconolite and powellite.

In order to study the structural changes of zirconolite crystals, Rietveld refinement of CTZ-30, CTZ-40 and CTZ-50 was performed using the JCPDS database [37–39]. Because three phases, zirconolite, powellite and perovskite, are detected in the XRD, multiple crystals are calculated simultaneously in the Rietveld refinement. The Rietveld refinement results are reported. As presented in Figure 4, the errors R_{wp} of CTZ-30, CTZ-40 and CTZ-50 between Y_{obs} and Y_{calc} are 7.43%, 9.20% and 7.80%, which are within the acceptable limits. Tables 2 and 3 list the refined cell parameters of zirconolite and powellite crystals, respectively. It is interesting that the cell parameters of powellite have little changes with the increase in CTZ content, while with the increasing content of CTZ, the cell volume of zirconolite firstly increases and then decreases. The results indicate that different amounts of Nd^{3+} cations have entered the lattice of zirconolite. This is because the radius of Nd^{3+} (1.109 Å) is similar to that of Ca^{2+} (1.12 Å) in 8-fold coordination, which enables Nd^{3+} to replace Ca^{2+} sites [40] and Ti^{4+} replaced by Al^{3+} cations to compensate charge as the following formula $\text{Ca}_{1-x}\text{Nd}_x\text{ZrTi}_{2-x}\text{Al}_x\text{O}_7$ [41,42]. It is interesting that there are two obvious

changes which can explain the changes in cell volume. One is the disappearance of surface crystallization. According to crystallography, one of the conditions for crystal precipitation is supersaturation of the solution. When there is a large amount of glass phase in the sample such as CTZ-30, Nd^{3+} is mainly dissolved into the glass first; when the glass phase in the sample decreases, such as CTZ-40, more Nd^{3+} cations enter its lattice in the process of zirconolite crystallization. The other is attributed to the appearance of perovskite. Nd^{3+} cations also can enter the lattice of perovskite during crystallization [43], which results in the crystals that immobilize Nd not being unique. Table S1 shows the detailed space occupying the results of zirconolite in the refined CTZ-40. According to the refinement results, zirconolite in CTZ-40 can be identified as $\text{Ca}_{0.78}\text{Nd}_{0.22}\text{ZrTi}_{1.78}\text{Al}_{0.22}\text{O}_7$.

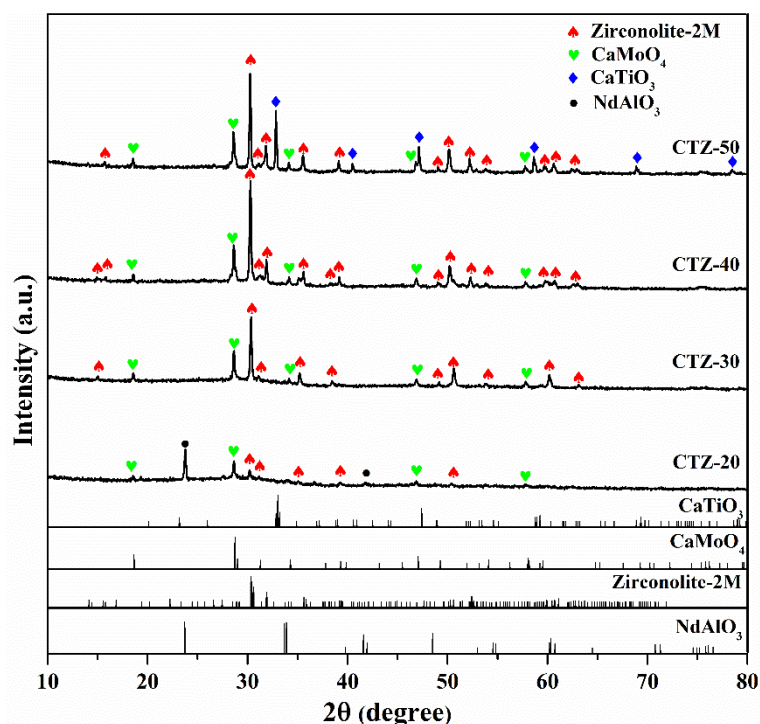


Figure 3. XRD patterns of glass-ceramics: CTZ-20, CTZ-30, CTZ-40 and CTZ-50.

Figure 5 shows the appearance of the glass-ceramic samples. CTZ-20 shows a slight purple glass sheen with a little split-phase. Figure 5b exhibits the appearance of CTZ-30, in which the amorphous phase is surrounded by a white crystal layer. Surface crystallization can be obviously observed for both CTZ-20 and CTZ-30. This is because the insufficient content of CTZ led to the low content of the crystalline phase, and crystallization started at the surface due to the high energy at the interface. As for the CTZ-40 and CTZ-50 samples shown in Figure 5c,d, the overall color and texture are consistent. It is obvious that the homogeneity is better. It is important to avoid uneven crystallization, which can lead to the uneven distribution of elements in the glass and crystalline layers, thus affecting the entry of the simulated nuclides into the crystals. The phenomenon indicates that increasing the CTZ content not only promotes more crystals, but it also leads to a more homogeneous waste form. Combined with the XRD pattern, these results indicate that the CTZ-40 sample is the most likely of these glass-ceramic samples to be used for HLW immobilization.

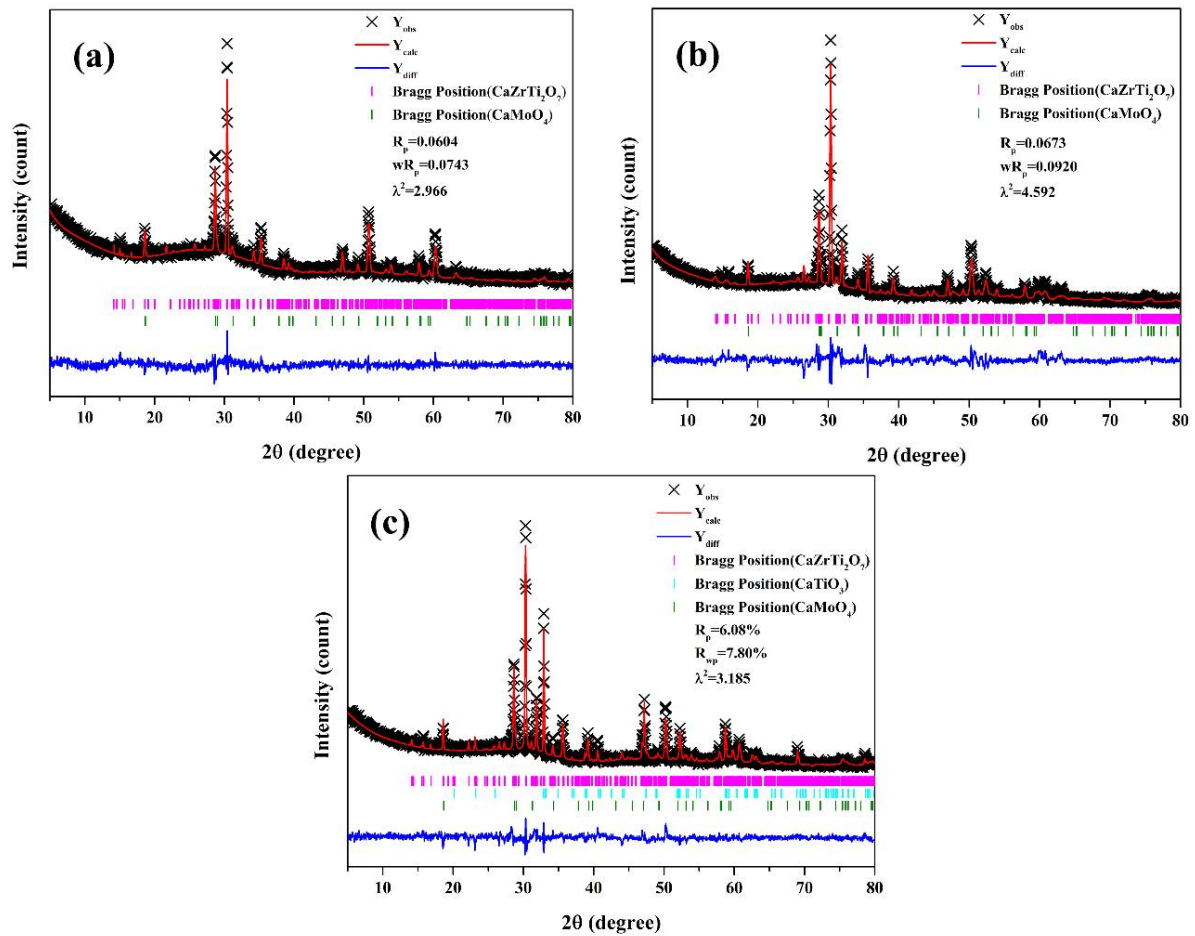


Figure 4. Rietveld refinement data map of the XRD of (a) CTZ-30, (b) CTZ-40 and (c) CTZ-50.

Table 2. Cell parameters obtained by refining the zirconolite phase in the obtained glass-ceramics. Numbers presented in parentheses are error standard deviations of the corresponding parameters.

Parameters	Raw Lattice	CTZ-30	CTZ-40	CTZ-50
a(Å)	12.4458	12.5298(4)	12.7909(1)	12.6149(4)
b(Å)	7.2734	7.2264(2)	7.3946(4)	7.2780(9)
c(Å)	11.3942	11.9817(4)	11.6172(1)	11.4489(3)
$\alpha(^{\circ})$	90.000	90.000(0)	90.000(0)	90.000(0)
$\beta(^{\circ})$	100.533	100.095(2)	100.900(6)	100.697(2)
$\gamma(^{\circ})$	90.000	90.000(0)	90.000(0)	90.000(0)
V(Å ³)	1014.06	1068.09(2)	1078.97(8)	1032.86(6)

Table 3. Cell parameters obtained by refining the powellite phase in the obtained glass-ceramics. Numbers presented in parentheses are error standard deviations of the corresponding parameters.

Parameters	Raw Lattice	CTZ-30	CTZ-40	CTZ-50
a(Å)	5.226	5.241(8)	5.249(10)	5.237(1)
b(Å)	5.226	5.241(8)	5.249(10)	5.237(1)
c(Å)	11.43	11.49(2)	11.49(2)	11.47(1)
$\alpha(^{\circ})$	90.0	90.0(0)	90.0(0)	90.0(0)
$\beta(^{\circ})$	90.0	90.0(0)	90.0(0)	90.0(0)
$\gamma(^{\circ})$	90.0	90.0(0)	90.0(0)	90.0(0)
V(Å ³)	312.17	315.48(6)	316.59(9)	314.62(2)

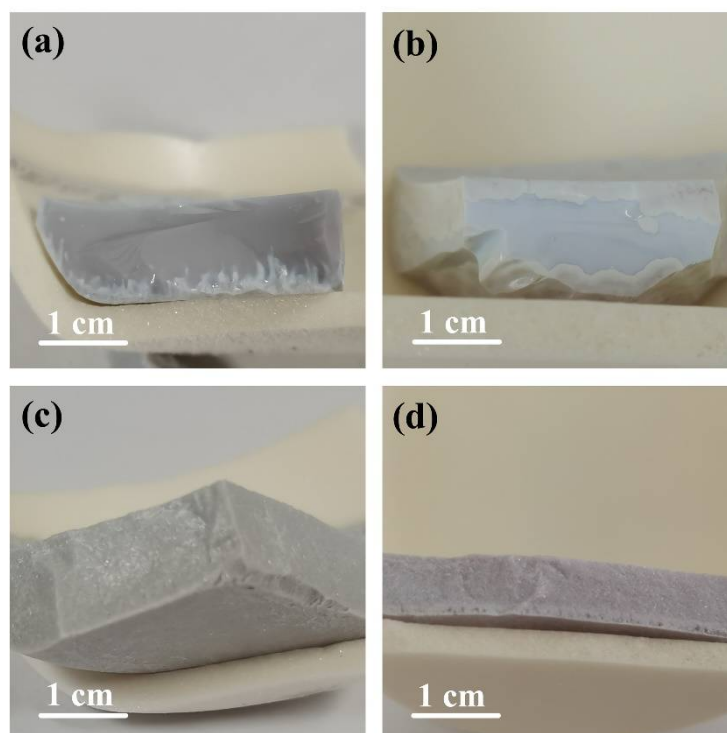


Figure 5. Appearance of the glass-ceramics: (a) CTZ-20; (b) CTZ-30; (c) CTZ-40 and (d) CTZ-50.

Figure 6 presents SEM micrographs of the glass-ceramics and the EDS spectra of the apparent crystals in the glass matrix. As shown in the appearance results, the CTZ-20 and CTZ-30 samples show obvious phase separation (Figure 6a,b). Figure 6e,f shows a microstructure at the interface between the crystallization zone and glass phase in the CTZ-20 and CTZ-30 samples. It can be observed that many zirconolite crystal clusters are immersed in the glass matrix, and the sizes of these crystals in the clusters are about 500 nm. Similar results have been observed in zirconolite-containing borosilicate glass-ceramics [44]. This phenomenon indicated that the content of CaO, TiO₂ and ZrO₂ is not enough to promote zirconolite crystallization in borosilicate glass. In addition, some spherical-shaped crystals in the glass matrix for the CTZ-30 samples were observed, which corresponds to the powellite phase [45]. This is the result of MoO₄²⁻ units separating from the glass network and then compensating the charge with Ca²⁺ cations [17,46]. It can be observed in Figure 6c,d that the CTZ-40 and CTZ-50 samples possess needle-shaped crystals with a size of about 60–90 μm in length, which is consistent with the previous work [47]. According to EDS analysis, the needle-shaped crystals correspond to zirconolite (Figure 6g). In addition, powellite crystals are mainly distributed around zirconolite crystals. However, some flaky crystals can be observed in the CTZ-50 samples. This should be related to perovskite crystallization according to EDS analysis (Figure 6h). The results obtained above indicate that the phase assemblage and microstructure of the multi-phase glass-ceramics are closely related to the content of CTZ in the glass and that the CTZ-40 sample is a candidate glass-ceramic for HLW immobilization.

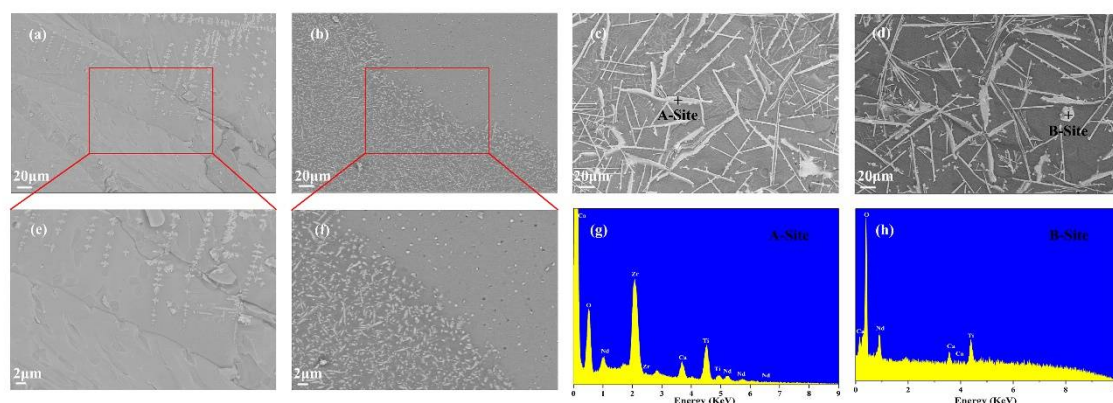


Figure 6. SEM images of the samples with different CTZ content: (a) CTZ-20, (b) CTZ-30, (c) CTZ-40, (d) CTZ-50; (e) partial enlarged view of CTZ-20, (f) partial enlarged view of CTZ-30; EDS spectra of CTZ-40 and CTZ-50: (g) A-Site, (h) B-Site.

In order to study the distribution of elements, elemental mapping was performed. Elemental mapping images of the CTZ-40 sample are shown in Figure 7. Ca, Ti and Zr elements were mainly concentrated in the needle-shaped zirconolite crystals, apparently. The Nd element was mainly distributed in the zirconolite crystals. The Mo element was mainly distributed in the powellite crystals. These results further indicate that Nd^{3+} cations entered into the lattice of zirconolite. Mo^{6+} cations mainly exist in the form of powellite and some of them dissolve in glass, which avoids the production of soluble molybdate.

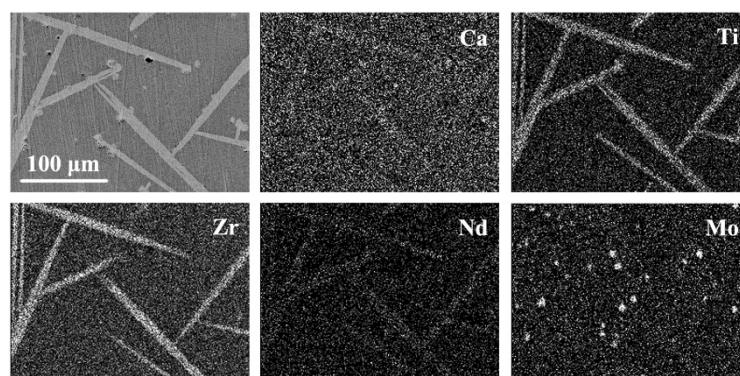


Figure 7. EDS maps of the typical CTZ-40 sample.

Bulk densities and molar volumes of the obtained glass-ceramic samples are presented in Figure 8. The densities of the samples are about 2.92, 3.05, 3.24 and 3.34 $\text{g}\cdot\text{cm}^{-3}$. Bulk densities of the glass-ceramics show an increasing trend with increasing CTZ content. In addition, molar volumes decreased from 25.77 to 24.44 $\text{cm}^3\cdot\text{mol}^{-1}$. Based on Table 1, the mean molar mass increased from 75.25 to 81.68 $\text{g}\cdot\text{mol}^{-1}$ with increasing CTZ content from 20 wt% to 50 wt%, which explains the increase in density.

Figure 9 presents the normalized leaching rates of Na (LR_{Na}), Ca (LR_{Ca}), Mo (LR_{Mo}) and Nd (LR_{Nd}) of the CTZ-40 samples. It can be observed that LR_{Na} , LR_{Ca} , LR_{Mo} and LR_{Nd} show a decreasing tendency with the increasing leaching time and tend to hold steady after 14 days. In previous studies [48–51], Si reacted with water as $\text{Si-O-Si} + \text{H}_2\text{O} \rightarrow \text{Si-O-H} + \text{HO-Si}$ led to a dense amorphous gel layer on the surface of the sample, as a diffusion barrier, which can be used to explain the decrease of normalized leaching rates. In addition, it can be observed in Figure 9 that for CTZ-40 samples, LR_{Na} and LR_{Ca} remained almost unchanged after 14 days at around $2.2 \times 10^{-3} \text{ g}\cdot\text{m}^{-2}\cdot\text{d}^{-1}$ and $7.2 \times 10^{-4} \text{ g}\cdot\text{m}^{-2}\cdot\text{d}^{-1}$, which is lower than that of the zirconolite glass-ceramics reported by Wu [52]. Furthermore, LR_{Mo} and LR_{Nd} also presented a downward trend with the increasing leaching time. For the typical CTZ-40 sample, LR_{Mo} and LR_{Nd} were about $6.4 \times 10^{-3} \text{ g}\cdot\text{m}^{-2}\cdot\text{d}^{-1}$ and $7.6 \times 10^{-5} \text{ g}\cdot\text{m}^{-2}\cdot\text{d}^{-1}$ at 28 d, which is generally lower than that of the powellite glass-

ceramics reported by Neeway [22] and the zirconolite glass-ceramics reported by Zhu [47], respectively. It can be further demonstrated that the zirconolite- and powellite-based multi-phase borosilicate glass-ceramics, especially the sample of CTZ-40 in this study, have suitable chemical durability.

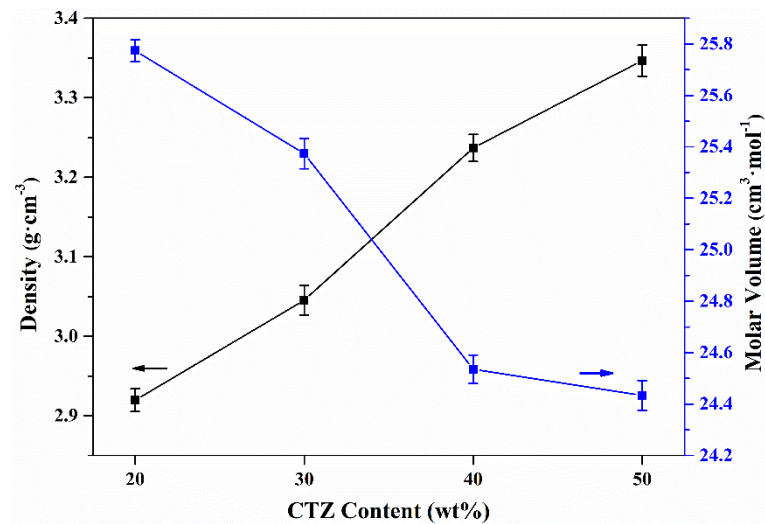


Figure 8. Bulk densities and molar volumes of the glass-ceramic samples.

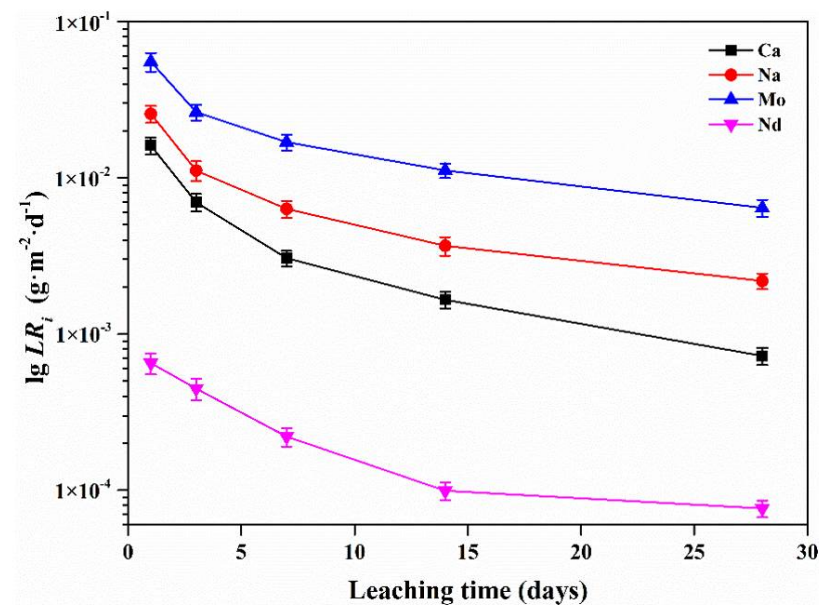


Figure 9. Normalized leaching rates of Na, Ca, Mo and Nd.

4. Conclusions

The multi-phase borosilicate glass-ceramics containing zirconolite and powellite with different CTZ content were synthesized for RE- and Mo-rich HLW immobilization by in situ thermal treatment. All RE and Mo in 35 wt% HLW were considered, where RE were all substituted by Nd. The effects of CTZ content on crystallization, microstructure and chemical durability were investigated. The results show that only the target crystal phases of zirconolite and powellite were detected in CTZ-40. For the CTZ-20 and CTZ-30 samples, insufficient CTZ content resulted in obvious crystallization on the surface of the samples. However, when the CTZ content increased to 50 wt%, a perovskite phase appeared. These results indicate that increasing the CTZ content can promote crystallization. For the typical CTZ-40 sample, zirconolite can be identified as $\text{Ca}_{0.78}\text{Nd}_{0.22}\text{ZrTi}_{1.78}\text{Al}_{0.22}\text{O}_7$, which

indicates that some Nd³⁺ cations entered the lattice of zirconolite. In addition, SEM and EDS analysis further confirmed the enrichment of Nd and Mo in the two target phases of zirconolite and powellite. Furthermore, the aqueous durability of the samples with different CTZ content is appropriate. For the typical CTZ-40 sample, LR_{Na} , LR_{Ca} , LR_{Mo} and LR_{Nd} were $2.2 \times 10^{-3} \text{ g}\cdot\text{m}^{-2}\cdot\text{d}^{-1}$, $7.2 \times 10^{-4} \text{ g}\cdot\text{m}^{-2}\cdot\text{d}^{-1}$, $6.4 \times 10^{-3} \text{ g}\cdot\text{m}^{-2}\cdot\text{d}^{-1}$ and $7.6 \times 10^{-5} \text{ g}\cdot\text{m}^{-2}\cdot\text{d}^{-1}$ at 28 d, respectively. The above preliminary research suggests that multi-phase borosilicate glass-ceramics containing zirconolite and powellite are potential waste forms for RE- and Mo-rich HLW immobilization.

Supplementary Materials: The following are available online at <https://www.mdpi.com/article/10.3390/ma14195747/s1>, Table S1: Structural Rietveld refinement results of the Nd-doped zirconolite phase for CTZ-40 sample.

Author Contributions: Methodology, formal analysis, investigation, writing-original draft, W.W.; conceptualization, supervision, Y.Z.; resources, formal analysis, writing-review and editing, X.Z.; formal analysis, D.Y.; validation, Y.H.; data curation, C.X.; validation, H.Y.; software, J.Z.; validation, resources, J.H.; investigation B.M. All authors have read and agreed to the published version of the manuscript.

Funding: This research was funded by the National Natural Science Foundation of China, [grant number 11702268], Longshan academic talent research supporting program of Southwest University of Science and Technology, China [grant number 18LZX560 and 18LZXT10], pre-research fund project of national defense key discipline laboratory of nuclear waste and environmental Safety Major China [grant number 17kfhk03] Science and Technology Special Project of Advanced Materials in Sichuan Province, China [grant number 2019ZDZX0023] and State Key Laboratory of Environmentally Friendly Energy Materials Project, China, [grant number 18FKSY0211].

Institutional Review Board Statement: Not applicable.

Informed Consent Statement: Not applicable.

Data Availability Statement: Not applicable.

Conflicts of Interest: The authors declare that they have no known competing financial interests or personal relationships that could have appeared to influence the work reported in this paper.

References

1. Crum, J.V.; Turo, L.; Riley, B.; Tang, M.; Kossoy, A. Multi-Phase Glass-Ceramics as a Waste Form for Combined Fission Products: Alkalis, Alkaline Earths, Lanthanides, and Transition Metals. *J. Am. Ceram. Soc.* **2012**, *95*, 1297–1303. [[CrossRef](#)]
2. Caurant, D.; Majerus, O.; Loiseau, P.; Bardez, I.; Baffier, N.; Dussossoy, J. Crystallization of neodymium-rich phases in silicate glasses developed for nuclear waste immobilization. *J. Nucl. Mater.* **2006**, *354*, 143–162. [[CrossRef](#)]
3. Laura, R.-P.; Soria, B.Y.M. A Review of the Nuclear Fuel Cycle Strategies and the Spent Nuclear Fuel Management Technologies. *Energies* **2017**, *10*, 1235.
4. Goel, A.; McCloy, J.S.; Pokorny, R.; Kruger, A.A. Challenges with vitrification of Hanford High-Level Waste (HLW) to borosilicate glass—An overview. *J. Non-Cryst. Solids X* **2019**, *4*, 100033. [[CrossRef](#)]
5. Goel, A.; McCloy, J.S.; Fox, K.M.; Leslie, C.J.; Riley, B.J.; Rodriguez, C.P.; Schweiger, M.J. Structural analysis of some sodium and alumina rich high-level nuclear waste glasses. *J. Non-Cryst. Solids* **2011**, *358*, 674–679. [[CrossRef](#)]
6. McCloy, J.S.; Marcial, J.; Patil, D.; Saleh, M.; Ahmadzadeh, M.; Chen, H.; Crum, J.V.; Riley, B.J.; Kamat, H.; Bréhault, A.; et al. Glass structure and crystallization in boro-alumino-silicate glasses containing rare earth and transition metal cations: A US-UK collaborative program. *MRS Adv.* **2019**, *4*, 1029–1043. [[CrossRef](#)]
7. Walling, S.A.; Kauffmann, M.N.; Gardner, L.J.; Bailey, D.J.; Stennett, M.C.; Corkhill, C.L.; Hyatt, N.C. Characterisation and disposability assessment of multi-waste stream in-container vitrified products for higher activity radioactive waste. *J. Hazard. Mater.* **2020**, *401*, 123764. [[CrossRef](#)] [[PubMed](#)]
8. McKeown, D.A.; Gan, H.; Pegg, I.L. X-ray absorption and Raman spectroscopy studies of molybdenum environments in borosilicate waste glasses. *J. Nucl. Mater.* **2017**, *488*, 143–149. [[CrossRef](#)]
9. Taurines, T.; Boizot, B. Synthesis of powellite-rich glasses for high level waste immobilization. *J. Non-Cryst. Solids* **2011**, *357*, 2723–2725. [[CrossRef](#)]
10. Crum, J.V.; Neeway, J.J.; Riley, B.; Zhu, Z.; Olszta, M.J.; Tang, M. Dilute condition corrosion behavior of glass-ceramic waste form. *J. Nucl. Mater.* **2016**, *482*, 1–11. [[CrossRef](#)]
11. Kossoy, A.; Schulze, R.; Tang, M.; Safarik, D.; McCabe, R. Nd–Mo-borosilicate glass–ceramic: Synthesis, characterization and response to ionizing radiation. *J. Nucl. Mater.* **2013**, *437*, 216–221. [[CrossRef](#)]

12. Caurant, D.; Majérus, O.; Fadel, E.; Quintas, A.; Gervais, C.; Charpentier, T.; Neuville, D. Structural investigations of borosilicate glasses containing MoO₃ by MAS NMR and Raman spectroscopies. *J. Nucl. Mater.* **2010**, *396*, 94–101. [[CrossRef](#)]
13. Patil, D.; Konale, M.; Gabel, M.; Neill, O.K.; Crum, J.V.; Goel, A.; Stennett, M.C.; Hyatt, N.C.; McCloy, J.S. Impact of rare earth ion size on the phase evolution of MoO₃-containing aluminoborosilicate glass-ceramics. *J. Nucl. Mater.* **2018**, *510*, 539–550. [[CrossRef](#)]
14. Boué, E.; Schuller, S.; Toplis, M.; Charpentier, T.; Mesbah, A.; Pablo, H.; Monnereau, M.; Moskura, M. Kinetic and thermodynamic factors controlling the dissolution of molybdate-bearing calcines during nuclear glass synthesis. *J. Nucl. Mater.* **2019**, *519*, 74–87. [[CrossRef](#)]
15. Chouard, N.; Caurant, D.; Majérus, O.; Dussossoy, J.-L.; Ledieu, A.; Peugeot, S.; Baddour-Hadjean, R.; Pereira-Ramos, J.-P. Effect of neodymium oxide on the solubility of MoO₃ in an aluminoborosilicate glass. *J. Non-Cryst. Solids* **2011**, *357*, 2752–2762. [[CrossRef](#)]
16. Chouard, N.; Caurant, D.; Majérus, O.; Guezi-Hasni, N.; Dussossoy, J.L.; Baddour-Hadjean, R.; Pereira-Ramos, J.P. Thermal stability of SiO₂-B₂O₃-Al₂O₃-Na₂O-CaO glasses with high Nd₂O₃ and MoO₃ concentrations. *J. Alloy. Compd.* **2016**, *671*, 84–99. [[CrossRef](#)]
17. Caurant, D.; Majerus, O.; Fadel, E.; Lenoir, M.; Gervais, C.; Pinet, O. Effect of molybdenum on the structure and on the crystallization of SiO₂-Na₂O-CaO-B₂O₃ glasses. *J. Am. Ceram. Soc.* **2007**, *90*, 774–783. [[CrossRef](#)]
18. Nicoleau, E.; Schuller, S.; Angeli, F.; Charpentier, T.; Jollivet, P.; Le Gac, A.; Fournier, M.; Mesbah, A.; Vasconcelos, F. Phase separation and crystallization effects on the structure and durability of molybdenum borosilicate glass. *J. Non-Cryst. Solids* **2015**, *427*, 120–133. [[CrossRef](#)]
19. Pinet, O.; Dussossoy, J.; David, C.; Fillet, C. Glass matrices for immobilizing nuclear waste containing molybdenum and phosphorus. *J. Nucl. Mater.* **2008**, *377*, 307–312. [[CrossRef](#)]
20. Brehault, A.; Patil, D.; Kamat, H.; Youngman, R.E.; Thirion, L.M.; Mauro, J.C.; Corkhill, C.L.; McCloy, J.S.; Goel, A. Compositional Dependence of Solubility/Retention of Molybdenum Oxides in Aluminoborosilicate-Based Model Nuclear Waste Glasses. *J. Phys. Chem. B* **2018**, *122*, 1714–1729. [[CrossRef](#)]
21. Peterson, J.A.; Crum, J.V.; Riley, B.J.; Asmussen, R.M.; Neeway, J.J. Synthesis and characterization of oxyapatite [Ca₂Nd₈(SiO₄)₆O₂] and mixed-alkaline-earth powellite [(Ca,Sr,Ba)MoO₄] for a glass-ceramic waste form. *J. Nucl. Mater.* **2018**, *510*, 623–634. [[CrossRef](#)]
22. Neeway, J.J.; Asmussen, R.M.; McElroy, E.M.; Peterson, J.A.; Riley, B.J.; Crum, J.V. Kinetics of oxyapatite [Ca₂Nd₈(SiO₄)₆O₂] and powellite [(Ca,Sr,Ba)MoO₄] dissolution in glass-ceramic nuclear waste forms in acidic, neutral, and alkaline conditions. *J. Nucl. Mater.* **2019**, *515*, 227–237. [[CrossRef](#)]
23. Asmussen, R.M.; Neeway, J.J.; Kaspar, T.C.; Crum, J.V. Corrosion Behavior and Microstructure Influence of Glass-Ceramic Nuclear Waste Forms. *Corrosion* **2017**, *73*, 1306–1319. [[CrossRef](#)]
24. McCloy, J.S.; Goel, A. Glass-ceramics for nuclear-waste immobilization. *MRS Bull.* **2017**, *42*, 233–240. [[CrossRef](#)]
25. Xu, A.; Wei, T.; Gregg, D.J.; Vance, E.R.; Zhang, Y.; Lumpkin, G.R. Micro-compression testing of gold ion irradiated zirconolite glass-ceramics as nuclear waste forms. *J. Nucl. Mater.* **2019**, *527*, 151813. [[CrossRef](#)]
26. Gupta, M.; Kulriya, P.K.; Shukla, R.; Dhaka, R.S.; Kumar, R.; Ghuman, S.S. Reduction and structural modification of zirconolite on He⁺ ion irradiation. *Nucl. Instrum. Methods Phys. Res. Sect. B Beam Interact. Mater. Atoms* **2016**, *379*, 119–125. [[CrossRef](#)]
27. Blackburn, L.R.; Sun, S.; Gardner, L.J.; Maddrell, E.R.; Stennett, M.C.; Hyatt, N.C. A systematic investigation of the phase assemblage and microstructure of the zirconolite CaZr_{1-x}Ce_xTi₂O₇ system. *J. Nucl. Mater.* **2020**, *535*, 152137. [[CrossRef](#)]
28. Blackburn, L.R.; Bailey, D.J.; Sun, S.-K.; Gardner, L.J.; Stennett, M.C.; Corkhill, C.L.; Hyatt, N.C. Review of zirconolite crystal chemistry and aqueous durability. *Adv. Appl. Ceram.* **2021**, *120*, 69–83. [[CrossRef](#)]
29. Wu, L.; Li, Y.; Teng, Y.; Meng, G. Preparation and characterization of borosilicate glass-ceramics containing zirconolite and titanite crystalline phases. *J. Non-Cryst. Solids* **2013**, *380*, 123–127. [[CrossRef](#)]
30. Loiseau, P.; Caurant, D. Glass-ceramic nuclear waste forms obtained by crystallization of SiO₂-Al₂O₃-CaO-ZrO₂-TiO₂ glasses containing lanthanides (Ce, Nd, Eu, Gd, Yb) and actinides (Th): Study of the crystallization from the surface. *J. Nuclear Mater.* **2010**, *402*, 38–54. [[CrossRef](#)]
31. Lv, P.; Chen, L.; Zhang, B.; Zhang, D.; Yuan, W.; Duan, B.; Guan, Y.; Pan, C.; Chen, Z.; Zhang, L.; et al. The effects of temperature and Ce-dopant concentration on the synthesis of zirconolite glass-ceramic. *Ceram. Int.* **2019**, *45*, 11819–11825. [[CrossRef](#)]
32. Li, H.; Wu, L.; Xu, D.; Wang, X.; Teng, Y.; Li, Y. Structure and chemical durability of barium borosilicate glass-ceramics containing zirconolite and titanite crystalline phases. *J. Nucl. Mater.* **2015**, *466*, 484–490. [[CrossRef](#)]
33. Zhang, K.; Yin, D.; Peng, L.; Wu, J. Self-propagating synthesis and CeO₂ immobilization of zirconolite-rich composites using CuO as the oxidant. *Ceram. Int.* **2017**, *43*, 1415–1423. [[CrossRef](#)]
34. ASTM C1285-14, *Standard Test Methods for Determining Chemical Durability of Nuclear, Hazardous, and Mixed Waste Glasses and Multiphase Glass Ceramics: The Product Consistency Test (PCT)*; ASTM: West Conshohocken, PA, USA, 2014.
35. Zhao, Z.; Chen, H.; Xiang, H.; Dai, F.-Z.; Wang, X.; Xu, W.; Sun, K.; Peng, Z.; Zhou, Y. High-entropy (Y_{0.2}Nd_{0.2}Sm_{0.2}Eu_{0.2}Er_{0.2})AlO₃: A promising thermal/environmental barrier material for oxide/oxide composites. *J. Mater. Sci. Technol.* **2020**, *47*, 45–51. [[CrossRef](#)]
36. Wang, X.; Wu, L.; Li, H.; Xiao, J.; Cai, X.; Teng, Y. Preparation and characterization of SO₃-doped barium borosilicate glass-ceramics containing zirconolite and barite phases. *Ceram. Int.* **2017**, *43*, 534–539. [[CrossRef](#)]
37. Rossell, H.J. Zirconolite—a fluorite-related superstructure. *Nature* **1980**, *283*, 282–283. [[CrossRef](#)]
38. Gürmen, E.; Daniels, E.; King, J.S. Crystal Structure Refinement of SrMoO₄, SrWO₄, CaMoO₄, and BaWO₄ by Neutron Diffraction. *J. Chem. Phys.* **1971**, *55*, 1093–1097. [[CrossRef](#)]

39. Beran, A.; Libowitzky, E.; Armbruster, T. A single-crystal infrared spectroscopic and X-ray diffraction study of untwinned San Benito perovskite containing O-H groups. *Can. Mineral.* **1996**, *34*, 803–809.
40. Loiseau, P.; Caurant, D.; Baffier, N.; Mazerolles, L.; Fillet, C. Glass–ceramic nuclear waste forms obtained from SiO₂–Al₂O₃–CaO–ZrO₂–TiO₂ glasses containing lanthanides (Ce, Nd, Eu, Gd, Yb) and actinides (Th): Study of internal crystallization. *J. Nucl. Mater.* **2004**, *335*, 14. [[CrossRef](#)]
41. Begg, B.D.; Vance, E.R. The incorporation of cerium in zirconolite. *Mater. Res. Soc.* **1997**, *465*, 333–340. [[CrossRef](#)]
42. Vance, E.; Ball, C.; Day, R.; Smith, K.; Blackford, M.; Begg, B.; Angel, P. Actinide and rare earth incorporation into zirconolite. *J. Alloy. Compd.* **1994**, *213–214*, 406–409. [[CrossRef](#)]
43. Wu, L.; Li, H.; Wang, X.; Xiao, J.; Teng, Y.; Li, Y. Effects of Nd Content on Structure and Chemical Durability of Zirconolite-Barium Borosilicate Glass-Ceramics. *J. Am. Ceram. Soc.* **2016**, *99*, 4093–4099. [[CrossRef](#)]
44. Liao, C.-Z.; Shih, K.; Lee, W.E. Crystal Structures of Al–Nd Codoped Zirconolite Derived from Glass Matrix and Powder Sintering. *Inorg. Chem.* **2015**, *54*, 7353–7361. [[CrossRef](#)]
45. Patel, K.B.; Peugeot, S.; Schuller, S.; Lampronti, G.I.; Facq, S.P.; Grygiel, C.; Monnet, I.; Farnan, I. Discovery of a maximum damage structure for Xe-irradiated borosilicate glass ceramics containing powellite. *J. Nucl. Mater.* **2018**, *510*, 229–242. [[CrossRef](#)]
46. Brinkman, K.; Fox, K.; Marra, J.; Reppert, J.; Crum, J.; Tang, M. Single phase melt processed powellite (Ba,Ca)MoO₄ for the immobilization of Mo-rich nuclear waste. *J. Alloy. Compd.* **2013**, *551*, 136–142. [[CrossRef](#)]
47. Zhu, H.; Wang, F.; Liao, Q.; Wang, Y.; Zhu, Y. Effect of CeO₂ and Nd₂O₃ on phases, microstructure and aqueous chemical durability of borosilicate glass-ceramics for nuclear waste immobilization. *Mater. Chem. Phys.* **2020**, *249*, 122936. [[CrossRef](#)]
48. Bunker, B.C.; Arnold, G.W.; Day, D.E.; Bray, P.J. The effect of molecular structure on borosilicate glass leaching. *J. Non-Cryst. Solids* **1986**, *87*, 226–253. [[CrossRef](#)]
49. Crawford, C.; Marra, J.; Bibler, N. Glass fabrication and product consistency testing of lanthanide borosilicate glass for plutonium disposition. *J. Alloy. Compd.* **2007**, *444–445*, 569–579. [[CrossRef](#)]
50. Martin, C.; Ribet, I.; Frugier, P.; Gin, S. Alteration kinetics of the glass-ceramic zirconolite and role of the alteration film—Comparison with the SON68 glass. *J. Nucl. Mater.* **2007**, *366*, 277–287. [[CrossRef](#)]
51. Rebiscoul, D.; Van der Lee, A.; Rieutord, F.; Né, F.; Spalla, O.; El-Mansouri, A.; Frugier, P.; Ayral, A.; Gin, S. Morphological evolution of alteration layers formed during nuclear glass alteration: New evidence of a gel as a diffusive barrier. *J. Nucl. Mater.* **2004**, *326*, 9–18. [[CrossRef](#)]
52. Wu, L.; Wang, X.; Li, H.; Teng, Y.; Peng, L. The effects of sulfate content on crystalline phase, microstructure, and chemical durability of zirconolite-barium borosilicate glass-ceramics. *J. Nucl. Mater.* **2016**, *478*, 303–309. [[CrossRef](#)]